Received: 7 November 2017 | Revised and accepted: 3 August 2018

DOI: 10.1002/jemt.23124

WILEY MICROSCOPY RESEARCH & TECHNIQUE

RESEARCH ARTICLE

Light sheet microscopy with high spatial resolution based on polarized structured illumination beam modulated by the phase mask

Levan Nhu[1,3] | Xiaona Wang[1] | Yong Liu[4] | Cuifang Kuang[1,2] | Xu Liu[1,2]

[1]State Key Laboratory of Modern Optical Instrumentation, College of Optical Science and Engineering, Zhejiang University, Hangzhou, China

[2]Collaborative Innovation Center of Extreme Optics, Shanxi University, Taiyuan, China

[3]Department of Optical Engineering, Le Quy Don Technical University, Hanoi, Vietnam

[4]Department of Electronic and Information Engineering, Shanghai University of Electric Power, Shanghai, China

Correspondence
Cuifang Kuang, State Key Laboratory of Modern Optical Instrumentation, Department of Optical Engineering, Zhejiang University, Hangzhou, China.
Email: cfkuang@zju.edu.cn

Funding information
National Key Research and Development Program of China, Grant/Award Number: 2016YFF0101400; National Basic Research Program of China (973Program), Grant/Award Number: 2015CB352003; National Natural Science Foundation of China (NSFC), Grant/Award Number: 61750110523, 61335003, 61427818; Natural Science Foundation of Zhejiang province, Grant/Award Number: LR16F050001; the Fundamental Research Funds for the Central Universities, Grant/Award Number: 2017FZA5004; Vietnam National Foundation for Science and Technology Development (NAFOSTED) under Grant, Grant/Award Number: 103.03-2018.08

Abstract

In this article, we present a method to improve axial resolution and expand the field of view of conventional light sheet fluorescence microscopy (LSFM) by phase modulation of the illumination beam. We added a bisected annular binary phase mask on the illumination path to modulate the radially polarized beam. The central spot of the modulated point spread function is narrower than that of Gaussian focus, although the sidelobe energy is increased. Then, a diffraction grating is used to produce multiple copies of this illumination pattern, and these pattern copies form the light sheet. By matching the numerical apertures of illumination lens and detection lens, the sidelobes on the detection axis can be suppressed in the captured data, although they do still contribute to photobleaching and phototoxicity in the sample. The simulation results show that the proposed method effectively reduces the thickness of the light sheet by 1.3 times, and increase the length of the light sheet by two times compared with conventional LSFM.

KEYWORDS

light sheet microscopy, structured illumination microscopy, superresolution

1 | INTRODUCTION

Three-dimensional (3D) live imaging is an important tool to understand biological processes. Many different techniques have been used for 3D imaging in recent years, such as confocal microscopy, wide-field microscopy, light sheet fluorescence microscopy (LSFM) and two-photon microscopy. Among them, LSFM is one of the fastest growing teniques (Ahrens, Orger, Robson, Li, & Keller, 2013; Fahrbach, Voigt, Schmid, Helmchen, & Huisken, 2013; Loic et al., 2016; Olarte, Andilla, Artigas, & Loza-Alvarez, 2015; Smyrek & Stelzer, 2017; Strnad et al., 2015; Tomer et al., 2015), because of its high speed, noninvasion and low photobleaching. In LSFM, there are two objective lenses whose optical axes are orthogonal to each other, so that the out-of-focus excitation is minimized. The illumination beam should be strictly confined to the focal plane of the detection lens to obtain clear images. LSFM has the following advantages: (a) quite low out-of-focus fluorescence background; (b) high imaging speed; (c) low photo-bleaching and photo-damage; and (d) high axial resolution.

There are two fundamental methods to generate the light sheet. In the first method, a cylindrical lens is used to focus the laser beam in one dimension to produce a light sheet. The light sheet produced by this method is also referred to as static light sheet, because the complete light sheet is formed instantaneously. Due to its simplicity, this method is very popular. In the second method, a single, thin laser beam is scanned across the plane by a laser scanner (galvo mirror) to produce a light sheet, which is called virtual light sheet.

Since the axial resolution of LSFM is determined by the thickness of light sheet, many efforts have been made to generate thinner light sheets. According to the principle of LSFM, the numerical aperture (NA) of the illumination lens determines the waist width of light sheet:

L.V. Nhu and Xiaona Wang contributed equally to this work.

the higher the NA, the thinner the light sheet. However, the higher the NA, the smaller the useful range of the light sheet, which means the narrower field of view. Therefore, there is a trade-off between the length and thickness of Gaussian light sheet. In order to produce longer and thinner light sheets simultaneously, some superresolution methods for confocal microscopy have been introduced in LSFM, such as stimulated emission depletion microscopy (Gohn-Kreuz & Rohrbach, 2016), structured illumination microscopy (SIM; Itoh, Landry, Hamann, & Solgaard, 2016), individual molecule localization (Gustavsson, Petrov, Lee, Shechtman, & Moerner, 2017), reversible saturable/switchable optical fluorescence transitions (Hoyer et al., 2016).

Phase modulation is a common technique to improve resolution in confocal scanning microscopy. For example, Toraldo-style phase mask (Francia, 1952) has been introduced in confocal scanning microscopy to produce the focus with a narrower central spot. Researchers have conducted theoretical researches on this phase mask in both paraxial limit (Gao, Gan, & Xu, 2007; Luo & Zhou, 2004; Reza & Hazra, 2013; Sheppard, Calvert, & Wheatland, 1998; Sheppard, Campos, Escalera, & Ledesma, 2008) and non-paraxial area (Kim, Bryant, & Stranick, 2012; Raghunathan & Potma, 2010). However, the energy in sidelobes would be increased if the Toraldo-style phase mask was used to modulate the excitation beam. Two methods have been proposed to solve this problem. In the first method, researchers coincide a second beam with the phase-modulated beam to eliminate sidelobes by the multi-beam nonlinear processes (Kim et al., 2012). In the second method, a spatial filter is introduced in the detection path to eliminate the effect of sidelobes. The pinhole in confocal scanning microscopy is a simple spatial filter, and the resolution of confocal scanning microscopy has been increased by 20% with this method (Le, Wang, Kuang, & Liu, 2018; Neil, Juškaitis, Wilson, Laczik, & Sarafis, 2000).

In this article, we introduce a phase mask in light sheet fluorescence microscopy, to improve axial resolution and enlarge field of view (FOV). Meanwhile, the introduction of bisected annular binary phase mask can also increase energy in sidelobes. To eliminate the effect of sidelobes, we choose the detection lens, whose NA matches that of illumination lens. The proposed method can effectively reduce the thickness of the light sheet by 1.3 times and increase the length of the light sheet by two times compared with the Gaussian light sheet.

2 | POLARIZED STRUCTURED ILLUMINATION BEAM MODULATED BY PHASE MASK

The focal effects of incident beam propagating through an objective lens can be calculated by vector diffraction theory. The electric field near the focus can be calculated by the formula derived from the Debye integral (Richards & Wolf, 1959):

$$\vec{E}(r_2,\varphi_2,z_2) = iC\iint_{\Omega} \sin(\theta) E_0 A(\theta,\varphi) P \times e^{i\Delta a(\theta,\varphi)} e^{ikn\left(z_2 \cos\theta + r_2 \sin\theta cons(\varphi-\varphi_2)\right)} d\theta d\varphi \quad (1)$$

where $\vec{E}(r_2,\varphi_2,z_2)$ is the electric field vector at the point (r_2, φ_2, z_2), which is expressed in cylindrical coordinates; C is a normalized constant; E_0 is the amplitude function of the input beam; $A(\theta, \varphi)$ is a 3 × 3 matrix related to the structure of the imaging lens; P is Jones vector of the incident beam; and $\Delta a(\theta, \varphi)$ is the parameter of phase delay generated by the phase mask.

When the objective lens satisfies the sine condition, $A(\theta, \varphi)$ can be presented by,

$$A(\theta,\varphi) = \sqrt{\cos\theta}\begin{bmatrix} 1+(\cos\theta-1)\cos^2\varphi & (\cos\theta-1)\cos\varphi\sin\varphi & -\sin\theta\cos\varphi \\ (\cos\theta-1)\cos\varphi\sin\varphi & 1+(\cos\theta-1)\sin^2\varphi & -\sin\theta\sin\varphi \\ \sin\theta\cos\varphi & \sin\theta\sin\varphi & \cos\theta \end{bmatrix} \quad (2)$$

When the incidence beam is spatially non-uniformly polarized, the radially polarized Jones vector is presented by,

$$\begin{pmatrix} p_x \\ p_y \\ p_z \end{pmatrix} = \begin{pmatrix} \cos\theta \\ \sin\theta \\ 0 \end{pmatrix} \quad (3)$$

The overall system point spread function (PSF) of LSFM can be calculated by multiplying the PSF of illumination lens and that of detection lens, which can be presented by,

$$PSF_{system}(x,y,z) = PSF_{Illu}(x,y,z) \times PSF_{Detec}(x,y,z) \quad (4)$$

where PSF_{system}, PSF_{Illu}, and PSF_{Detec} are the overall system PSF, the illumination PSF and the detection PSF, respectively.

In order to obtain an effective light sheet in LSFM, in this article, we propose to modulate radially polarized beam with a bisected annular binary phase mask to generate the illumination beam. The proposed shape of phase mask is shown in Figure 1. If we used the sweeping method to form the virtual light sheet, the sidelobes would affect the axial resolution of LSFM significantly. So we introduced a diffraction grating in the illumination path to produce multiple copies of the illumination pattern (Gao, Shao, Chen, & Betzig, 2014).

Next, we consider the intensity distributions when the radially polarized beam is modulated by the phase masks with different ratios of r2/r1. When NA of the illumination lens is set to 0.3, Figure 2 shows the intensity distributions at different K values (K = r2/r1), where K is set to 0, 0.2, 0.4, 0.6, and 0.8. As shown in Figure 2, the intensity distribution of the phase-modulated radially polarized beam is not radially symmetrical in the x–z plane: the sidelobes in the x direction are blocked, while they are not blocked in the z direction. It is not difficult to see that when K changes, the intensity distribution of the phase-modulated radially polarized beam also changes. As Figure 2a–d shows, when K is increasing, both the intensity and the size of sidelobes are increasing. However, the size of the central lobe is decreasing at the same time. In addition, the size of the entire beam is increasing, which causes extra bleaching and out-of-focus background. So we should choose a suitable value of K to balance the size of central lobes and the effects of sidelobes. It is worth noting that when K value is set to 0.8 (Figure 2e), the shape of the central lobe is a doughnut.

3 | SIMULATION RESULTS

In order to show the effectiveness of proposed method, we simulated with an illumination lens with 0.3 NA. The intensity distributions of the Gaussian beam and the phase-modulated radially polarized beam at sample are shown at the top and bottom of Figure 3a, respectively. As stated in Section 2, the phase-modulated radially polarized beam is

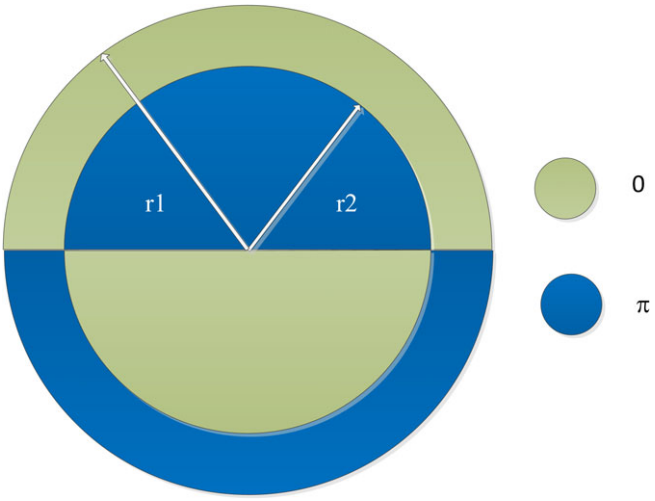

FIGURE 1 The bisected annular binary mask, which is used to modulate the radially polarized beam. This phase mask with radius r1 is divided into two parts from the middle. The phase is 0 on one side and π on another, and a π step occurs at radius r2 [Color figure can be viewed at wileyonlinelibrary.com]

formed by modulating radially polarized beam with a phase mask. The shape of this phase mask has also been mentioned in Section 2, and we set the value of parameter K to 0.45. As can be seen from Figure 3a, the section size of the phase-modulated radially polarized beam is bigger than that of the Gaussian beam. However, the size of the central lobe of the phase-modulated radially polarized beam is smaller than that of the Gaussian beam.

The Gaussian beam is swept quickly across the plane by a galvo mirror, to create a light sheet, which is called the Gaussian light sheet. In mathematical model, the Gaussian light sheet is obtained by integrating the PSF of the Gaussian beam, $PSF_{Gaussian}(x,y,z)$ along x direction, which can be presented by,

$$PSF_{Illu}(y,z) = \int PSF_{Gaussian}(x,y,z)dx \quad (5)$$

As presented in Section 2, in order to obtain the light sheet of phased-modulated radially polarized beam, a grating-based diffraction optical element is added to the optical system (Gao et al., 2014). The diffraction grating is used to produce multiple copies of the illumination pattern, so that a kind of light sheet, which is called the SIM light sheet, is created. In mathematical model, the SIM light sheet is achieved by the convolution of the PSF of the phased-modulated radially polarized beam, $PSF_{PM}(x,y,z)$, and a periodical modulation function, $M(x)$, in real space (Gao et al., 2014). It can be presented by,

$$PSF_{Illu}(x,y,z) = PSF_{PM}(x,y,z) \otimes M(x) \quad (6)$$

The cross-sectional intensity distribution of the Gaussian light sheet, which is calculated by Equation (5), is shown at the top of Figure 3b. The cross-sectional intensity distribution of the SIM light sheet, which is calculated by Equation (6), is shown at the bottom of Figure 3b. As can be seen from Figure 3b, the width of the central lobe of the SIM light sheet along z axial direction is narrower than that of the Gaussian light sheet. The intensity distributions of the SIM and Gaussian light sheets along z axis are shown in Figure 4. It can be seen clearly from Figure 4 that the full width at half maximum (FWHM) of the Gaussian light sheet is 1.3 times bigger than that of the SIM light sheet. This means that the SIM light sheet can produce images with higher axial resolution. In order to obtain a good result, the sidelobes of the SIM light sheet must be removed from the overall system PSF. This can be performed by multiplying both excitation and detection PSFs as stated in Section 2. By matching the NAs of the illumination and detection lenses, the sidelobes of the SIM light sheet are suppressed in the captured data (Chen et al., 2014). For the SIM light sheet shown at the bottom of Figure 3b, the optimal NA of detection lens is equal to 1.1. Both intensity distributions of the detection beam and the SIM light sheet along z-axis are shown in Figure 5. It can be

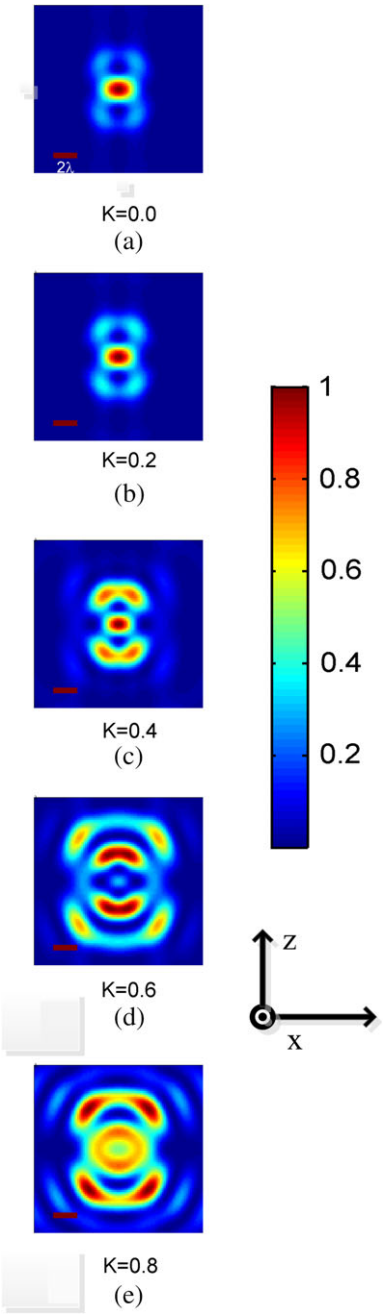

FIGURE 2 Intensity distributions of illumination patterns in the x–z plane at different K values (K = r2/r1, r1, r2 are shown in Figure 1.), K is set to 0, 0.2, 0.4, 0.6, and 0.8, respectively. The axes are shown on the right [Color figure can be viewed at wileyonlinelibrary.com]

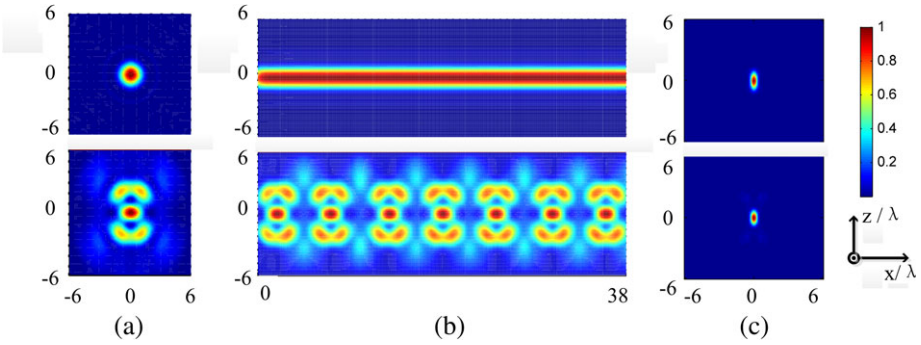

FIGURE 3 Conventional Gaussian light sheet at the top and structured illumination microscopy (SIM) light sheet at the bottom. (a) the intensity distributions of the pattern in the *x*–*z* plane at the focus of the illumination lens; (b) the intensity distribution of the light sheet created by scanning Gaussian beam along x direction and that of SIM light sheet; (c) the overall system PSFs in the *x*–*z* plane. PSF, point spread function [Color figure can be viewed at wileyonlinelibrary.com]

seen that the sidelobes of the SIM light sheet coincides with the position with low intensity of the detection beam, so that we can remove the sidelobes of the SIM light sheet in the overall system PSF.

We can get the overall system PSFs by multiplying both excitation and detection PSFs. The overall system PSFs of the Gaussian and SIM light sheets in *x*–*z* plane are depicted at the top and bottom of Figure 3c, respectively. The intensity distributions along *z*-axis are shown in Figure 6. As Figure 6 indicates, we can easily find that the axial resolution of the SIM light sheet is higher than that of the Gaussian light sheet.

The proposed method can also extend the field of view in LSFM. Figure 7 indicates the intensity distributions of the Gaussian and SIM light sheets in the *y*–*z* plane. The intensity distribution of the SIM light sheet in the *y*–*z* plane includes three parts: the one central lobe and both sidelobes. However, only the central part is used to obtain images, which means that the FOV of the SIM light sheet is calculated by the central lobe. As Figure 7 shows, the central lobe of the SIM light sheet is longer than that of the Gaussian light sheet. From Figure 8, we quantify the length of the Gaussian and SIM light sheets by drawing the intensity distribution of light sheets at the central peak position along *y*-axis. It can be seen that the length of the SIM light sheet is longer than that of the Gaussian light sheet. When the limit line is chosen at a value equal to 0.5, the SIM light sheet is about two times longer than the Gaussian light sheet.

In order to obtain final images of the SIM light sheet in each plane, the raw images should be processed. The processing method is similar to that used in conventional wide-field SIM. In conventional wide-field SIM, we can illuminate the sample with a periodic illumination pattern with period *T*, and obtain a series of raw images as the pattern moves *N* times in equal steps of *N*/*T*. When *N* raw images of the SIM light sheet are obtained, we can get a high-quality image by the digital processing. The digital processing method had been proven to be feasible in traditional SIM (Neil, Juškaitis, & Wilson, 1997), the *N* raw images, I_j, where j = 0, 1, …, and *N*−*1*, (*N* ≥ 3), are combined to acquire the high-quality image as:

$$I = \left| \sum_{j=0}^{N-1} I_j \exp(i2\pi j/N) \right| \tag{7}$$

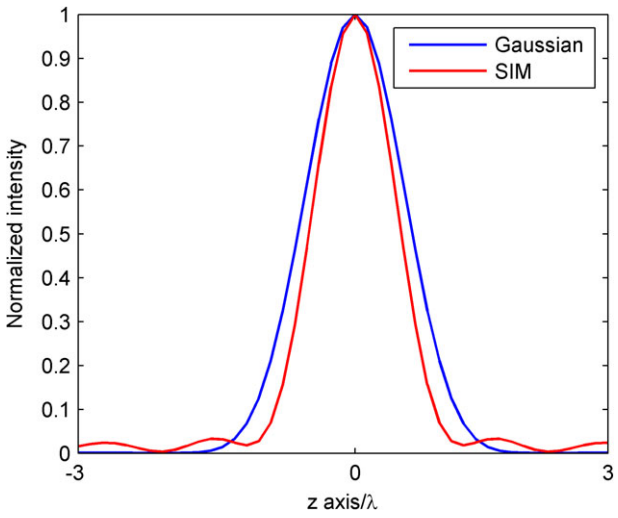

FIGURE 4 Illumination intensity distributions along z axis at the focus of the illumination lens: the blue line is Gaussian light sheet; the red one is SIM light sheet. SIM, structured illumination microscopy [Color figure can be viewed at wileyonlinelibrary.com]

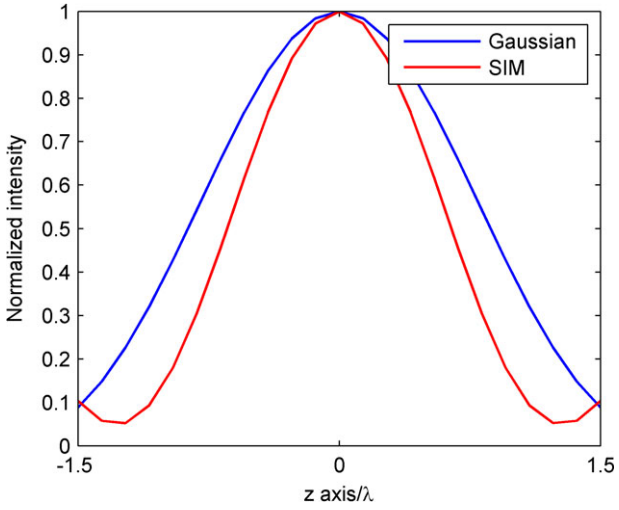

FIGURE 5 The intensity distributions of detection beam, structured illumination microscopy (SIM) light sheet and overall system point spread function (PSF) along *z*-axis: The green line is SIM light sheet, the blue one is detection lens, the red one is overall system PSF [Color figure can be viewed at wileyonlinelibrary.com]

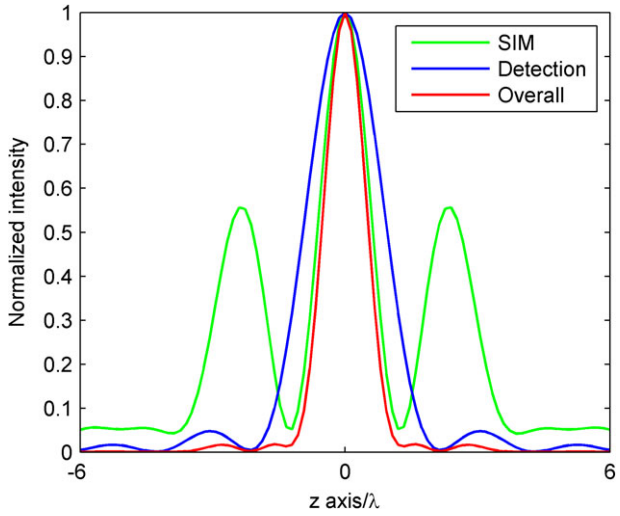

FIGURE 6 The intensity distributions of Gaussian light sheet and structured illumination microscopy (SIM) light sheet along *z*-axis: the blue line is Gaussian light sheet; the red one is SIM light sheet [Color figure can be viewed at wileyonlinelibrary.com]

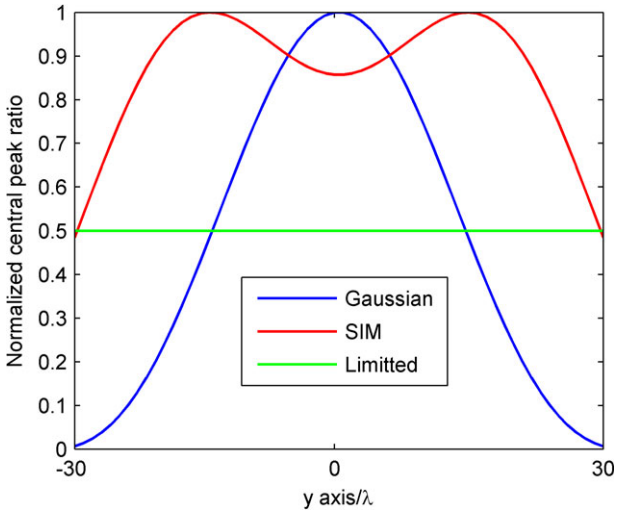

FIGURE 8 The intensity distributions of Gaussian light sheet and structured illumination microscopy (SIM) light sheet along *y*-axis. The blue line is Gaussian light sheet; the red one is SIM light sheet, the green line is the limit line whose value is set to 0.5 [Color figure can be viewed at wileyonlinelibrary.com]

To obtain high-quality image, the minimum number of raw images in each plane is equal to 3. For most samples in the SIM light sheet, *N* value should be set to 7 or 9. In addition, when the SIM processing algorithm is used to achieve final image, the out-of-focus background can be removed.

An optical system layout of the SIM light sheet is shown in Figure 9. In this layout, the galvo mirror, *G_x*, is used to control the movement of the SIM light sheet in *x* direction to obtain *N* raw images in each plane. Sample is moved along *z*-axis to obtain each stack.

As is known to all, Bessel light sheet is also a useful way to improve the axial resolution and enlarge the FOV (Chen et al., 2014). In here, we compare imaging performance of proposed SIM light sheet and Bessel light sheet in two conditions. The first condition, we have ensured that the area of the incident light beam in the pupil plane is the same. The NA of illumination lens used by Bessel beam is equal to 0.6. The cross-section of Bessel PSF is shown Figure 10a. The intensity distribution of Bessel light sheet along *z*-axis is shown in Figure 11c. The comparison of the overall system PSF excited by Bessel light sheet and SIM light sheet is shown in Figure 11a,b, respectively. Figure 12 shows the length of SIM light sheet and Bessel light sheet. As can be seen from Figure 12, the length of SIM light sheet is longer than that of Bessel light sheet. Additionally, the NA of illumination lens used by SIM light sheet is lower, which is 0.3, so the working distance of illumination lens of the proposed method can be longer. This is an advantage in the practical applications. Although the axial resolution of Bessel light sheet is better than that of SIM light sheet according to the FWHM in Figure 11c, the difference between them

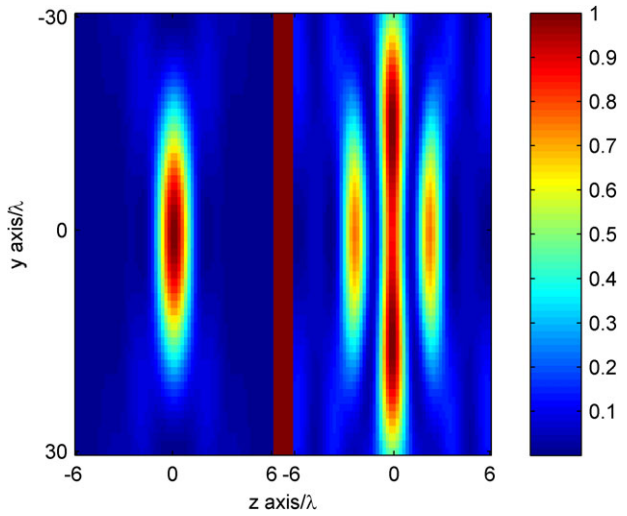

FIGURE 7 The intensity distributions of Gaussian light sheet and structured illumination microscopy (SIM) light sheet in *y*–*z* plane. The left figure is the Gaussian light sheet and the right one is SIM light sheet [Color figure can be viewed at wileyonlinelibrary.com]

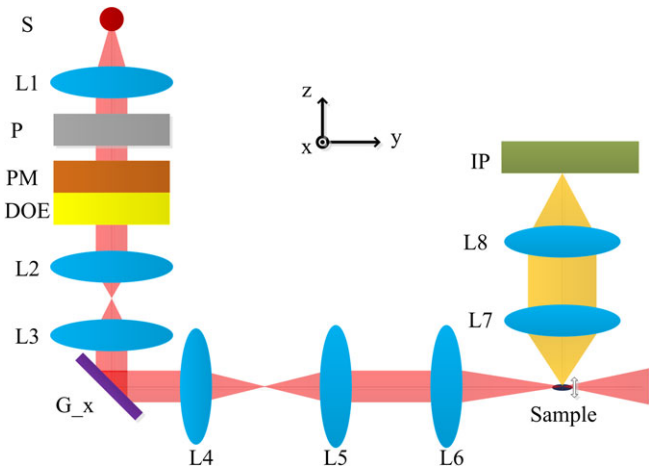

FIGURE 9 The optical system layout of the structured illumination microscopy (SIM) light sheet. S is laser source; L1–L5 are relay lenses; L6 is illumination lens; L7 is detection lens; L8 is a tube lens; P is a radial polarization plate; PM is a phase mask; DOE is a grating-based diffraction optical element, which is placed behind the phase mask; G_x is a galvo mirror which is used to control the shift of SIM light sheet along *x* direction to obtain *N* raw images on each plane; IP is detector [Color figure can be viewed at wileyonlinelibrary.com]

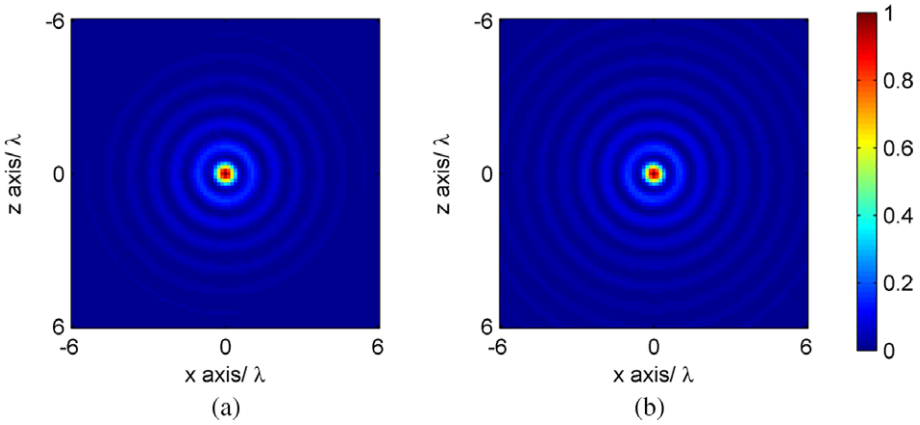

FIGURE 10 The cross-sectional intensity distributions of Bessel light sheet in *x*–*z* plane: (a) the Bessel light sheet has the same area in the pupil plane structured illumination microscopy (SIM) light sheet and (b) the Bessel light sheet has the same FOV in the pupil plane SIM light sheet. The unit of axes is wavelength. FOV, field of view [Color figure can be viewed at wileyonlinelibrary.com]

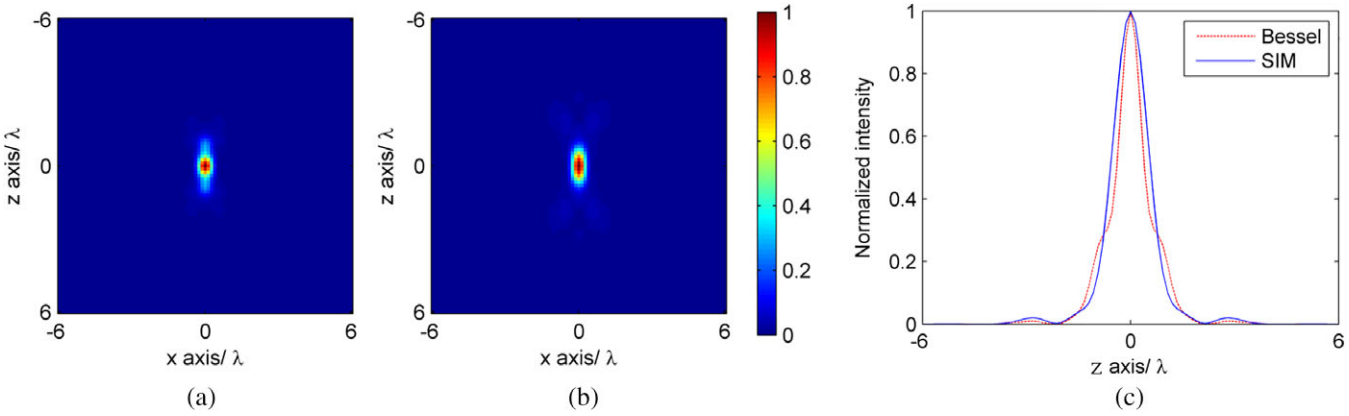

FIGURE 11 The intensity distributions of overall system point spread function (PSF) excited by Bessel light sheet (a) and structured illumination microscopy (SIM) light sheet (b) in *x*–*z* plane. The intensity distributions of overall system PSF excited by different light sheet along *z*-axis is shown in figure (c). The dotted red line is the distribution excited by Bessel light sheet; the blue one is the distribution excited by SIM light sheet [Color figure can be viewed at wileyonlinelibrary.com]

is slight. Besides, as Figure 11c shows, the intensity distribution of Bessel light sheet is stronger than that of SIM light sheet in a specific area, which might lead to more background of images in the *x*–*y* plane by using Bessel light sheet. In other words, the SIM light sheet has great advantages over Bessel light sheet, in the FOV, working distance and background. The second condition, the area of incident light beam in the pupil plane will shrink if we ensure that FOV of Bessel light sheet and SIM light sheet is the same. The intensity distribution of this Bessel beam is shown in Figure 10b. As Figure 10b shows, the shape of intensity distribution of Bessel beam near center is not changed and therefore the axial resolution can be kept (Olarte, Andilla, Emilio, & Pablo, 2018). However, the sidelobes become wider, which means increasing photobleaching and phototoxicity in the sample.

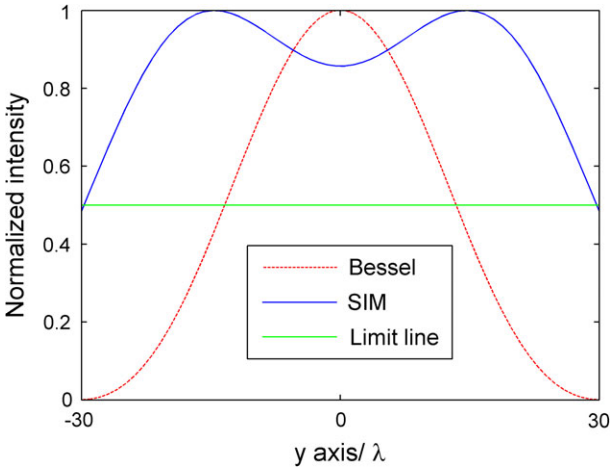

FIGURE 12 The intensity distributions of Bessel light sheet and structured illumination microscopy (SIM) light sheet along *y*-axis. The dotted red line is Bessel light sheet; the blue one is SIM light sheet, the green line is the limit line whose value is set to 0.5 [Color figure can be viewed at wileyonlinelibrary.com]

4 | CONCLUSION

In this article, we have demonstrated that the SIM light sheet can overcome the contradiction between the length and thickness in conventional LSFM. To modulate the radially polarized beam, we have

introduced a bisected annular binary phase mask. Then the diffraction grating is used to generate the SIM light sheet. The simulation results demonstrated that the proposed SIM light sheet can be used to obtain 1.3 times higher axial resolution and two times longer length compared with the conventional Gaussian light sheet. In the future, we will use this SIM light sheet to obtain 3D live imaging with higher axial resolution and wider FOV.

ACKNOWLEDGMENTS

This work is supported by The National Key Research and Development Program of China (2016YFF0101400); National Basic Research Program of China (973Program) (2015CB352003); National Natural Science Foundation of China (NSFC) (61750110523, 61335003, 61427818); and Natural Science Foundation of Zhejiang province (LR16F050001), the Fundamental Research Funds for the Central Universities (2017FZA5004), and Vietnam National Foundation for Science and Technology Development (NAFOSTED) under Grant (103.03-2018.08).

ORCID

Levan Nhu http://orcid.org/0000-0001-6893-4334

REFERENCES

Ahrens, M. B., Orger, M. B., Robson, D. N., Li, J. M., & Keller, P. J. (2013). Whole-brain functional imaging at cellular resolution using light-sheet microscopy. *Nature Methods*, *10*, 413–420.

Chen, B. C., Legant, W. R., Wang, K., Shao, L., Milkie, D. E., Davidson, M. W., … Betzig, E. (2014). Lattice light-sheet microscopy: Imaging molecules to embryos at high spatiotemporal resolution. *Science*, *346*, 1257998.

Fahrbach, F. O., Voigt, F. F., Schmid, B., Helmchen, F., & Huisken, J. (2013). Rapid 3D light-sheet microscopy with a tunable lens. *Optics Express*, *21*, 21010–21026.

Francia, G. (1952). Super-gain antennas and optical resolving power. *Il Nuovo Cimento.*, *9*, 426–438.

Gao, X., Gan, F., & Xu, W. (2007). Superresolution by three-zone pure phase plate with 0, π, 0 phase variation. *Optics and Laser Technology*, *39*, 1074–1080.

Gao, L., Shao, L., Chen, B.-C., & Betzig, E. (2014). "3D live fluorescence imaging of cellular dynamics using Bessel beam plane illumination microscopy." *Nature Protocols 9*(5), 1083–1101.

Gohn-Kreuz, C., & Rohrbach, A. (2016). Light sheet generation in inhomogeneous media using sekt-resontructing beams and the STED-principle. *Optics Express*, *24*(6), 5855.

Gustavsson. A. K, P. N. Petrov, M. Y. Lee, Y. Shechtman, W. E. Moerner. (2017). "3D single-molecule super-resolution microscopy with a tilted light sheet," *Nat Commun. 9*(1), 14a.

Hoyer, P., Medeiros, G. D., Balszs, B., Norlin, N., Besir, C., Hanne, J., Krausslich, H. G., Engellhardt, J., Sahl, S. J., Hell, S. W., HUfnagel, L. (2016). "Breaking the diffraction limit of light-sheet fluorescence microscopy by RESOLFT," *PNAS 113*(13), 3442–2446.

Itoh, R., Landry, J. R., Hamann, S. S., & Solgaard, O. (2016). Light sheet fluorescence microscopy using high-speed structured and pivoting illumination. *Optics Letters*, *41*(21), 5015–5018.

Kim, H., Bryant, G. W., & Stranick, S. J. (2012). Superresolution four-wave mixing microscopy. *Optics Express*, *20*, 6042–6051.

Le, V., Wang, X., Kuang, C., & Liu, X. (2018). "Resolution enhancement of confocal scanning microscopy using low-intensity imaging part of point spread function." *Optical Engineering 57*, 053156.

Loic, R., William, C. L., Raghav, K. C., Yinan, W., Michael, C., Eugene, W. M., & Philipp, J. K. (2016). Adaptive light sheet microscopy for long-term, high resolution imaging in living organisms. *Nature Biotechnology*, *34*(12), 1267–1281.

Luo, H., & Zhou, C. (2004). Comparison of superresolution effects with annular phase and amplitude filters. *Applied Optics*, *43*, 6242–6247.

Olarte, O. E., Andilla, J., Emilio, J. G., & Pablo, L. A. (2018). Light-sheet microscopy: A tutorial. *Advances of Optics and Photonics. 10*, 111.

Neil, M. A. A., Juškaitis, R., & Wilson, T. (1997). Method of obtaining optical sectioning by using structured light in a conventional microscope. *Optics Letters*, *22*, 1905–1907.

Neil, M. A. A., Juškaitis, R., Wilson, T., Laczik, Z. J., & Sarafis, V. (2000). Optimized pupil-plane filters for confocal microscope point-spread function engineering. *Optics Letters*, *25*, 245–247.

Olarte, E., Andilla, J., Artigas, D., & Loza-Alvarez, P. (2015). Decoupled illumination detection in light sheet microscopy for fast volumetric imaging. *Optica*, *2*, 702–705.

Raghunathan, V., & Potma, E. O. (2010). Multiplicative and subtractive focal volume engineering in coherent Raman microscopy. *Journal of the Optical Society of America*, *27*, 2365–2374.

Reza, N., & Hazra, L. (2013). Toraldo filters with concentric unequal annuli of fixed phase by evolutionary programming. *Journal of the Optical Society of America*, *30*, 189–195.

Richards, B., & Wolf, E. (1959). Electromagnetic diffraction in optical systems. 2. Structure of the image field in an aplanatic system. *Proceedings of the Royal Society of London A*, *253*, 358–379.

Sheppard, C., Calvert, G., & Wheatland, M. (1998). Focal distribution for superresolving toraldo filters. *Journal of the Optical Society of America*, *15*, 849–856.

Sheppard, C. J. R., Campos, J., Escalera, J. C., & Ledesma, S. (2008). Two-zone pupil filters. *Optics Communication*, *281*, 913–922.

Isabell, S., & Ernst, H. K. S. (2017). "Quantitative three-dimensional evaluation of immunofluorescence staining for large wholemount spheroids with light sheet microscopy." *Biomedial Optics Express 8*, 484–499.

Strnad, P., Gunther, S., Reichmann, J., Krzic, U., Balazs, B., de Medeiros, G., … Ellenberg, J. (2015). Inverted light-sheet microscope for imaging mouse pre-implantation development. *Nature Methods*, *13*, 139–142.

Tomer, R., Lovett-Barron, M., Kauvar, I., Andalman, A., Burns, V. M., Sankaran, S., … Deisseroth, K. (2015). SPED light sheet microscopy: Fast mapping of biological system structure and function. *Cell*, *163*, 1796–1806.

How to cite this article: Nhu L, Wang X, Liu Y, Kuang C, Liu X. Light sheet microscopy with high spatial resolution based on polarized structured illumination beam modulated by the phase mask. *Microsc Res Tech*. 2018;1–7. https://doi.org/10.1002/jemt.23124